Biochemical Indication for Myristoylation-Dependent Conformational Changes in HIV-1 Nef†

Sebastian Breuer,‡ Holger Gerlach,‡ Branko Kolaric,‡,§ Claus Urbanke,|| Norbert Opitz,‡ and Matthias Geyer*,‡

Abteilungen Physikalische Biochemie und Strukturelle Biologie, Max-Planck-Institut für Molekulare Physiology, Otto-Hahn-Strasse 11, 44227 Dortmund, Germany, and Biophysikalisch-Biochemische Verfahren, Medizinische Hochschule Hannover, Carl Neuberg Strasse 1, 30625 Hannover, Germany

Received October 9, 2005; Revised Manuscript Received December 28, 2005

ABSTRACT: The accessory HIV-1 Nef protein is essential for viral replication, high virus load, and progression to AIDS. These functions are mediated by the alteration of signaling and trafficking pathways and require the membrane association of Nef by its N-terminal myristoylation. However, a large portion of Nef is also found in the cytosol, in line with the observation that myristoylation is only a weak lipidation anchor for membrane attachment. We performed biochemical studies to analyze the implications of myristoylation on the conformation of Nef in aqueous solution. To establish an in vivo myristoylation assay, we first optimized the codon usage of Nef for *Escherichia coli* expression, which resulted in a 15-fold higher protein yield. Myristoylation was achieved by coexpression with the *N*-myristoyltransferase and confirmed by mass spectrometry. The myristoylated protein was soluble, and proton NMR spectra confirmed proper folding. Size exclusion chromatography revealed that myristoylated Nef appeared of smaller size than the unmodified form but not as small as an N-terminally truncated from of Nef that omits the anchor domain. Western blot stainings and limited proteolysis of both forms showed different recognition profiles and degradation pattern. Analytical ultracentrifugation revealed that myristoylated Nef prevails in a monomeric state while the unmodified form exists in an oligomeric equilibrium of monomer, dimer, and trimer associations. Finally, fluorescence correlation spectroscopy using multiphoton excitation revealed a shorter diffusion time for the lipidated protein compared to the unmodified form. Taken together, our data indicated myristoylation-dependent conformational changes in Nef, suggesting a rather compact and monomeric form for the lipidated protein in solution.

The covalent attachment of lipophilic moieties to cytosolic proteins is an important modification for the biological activity of many regulatory proteins. These lipidations serve in most cases as anchoring groups for targeting the proteins to a certain membrane or submembrane compartment. The most common hydrophobic modifications are fatty acids (myristate and palmitate), isoprenoids (farnesyl and geranylgeranyl), and glycosyl-phosphatidylinositol anchors (*1*). Stability and specificity for the association to particular membranes is often achieved by heterogeneous acylation of two or more lipid groups and combinations with charged or hydrophobic patches within the protein.

Nef[1] is an accessory protein of human and simian immunodeficiency viruses that is essential for viral replication, high virus load, and progression to AIDS (*2*). Viruses deleted in *nef* replicate with significantly reduced kinetics in vivo, resulting in asymptomatic infections of the host. On a molecular level three functions are subscribed to Nef: First, by interacting with tyrosine and serine/threonine kinases Nef alters cellular signaling pathways. Second, Nef increases viral infectivity at a step after the entry of the virus into the cell. Third, by interacting with components of the endocytic machinery, Nef decreases the expression of CD4 and major histocompatibility complex class I and II (MHC I and II) antigens on the surface of infected cells (for reviews see refs *3*−*5*). These functions require the association with many different proteins or multiprotein complexes to serve the multiple variable interactions subscribed to Nef. Recent findings identified the DOCK2−ELMO1 complex (*6*), a key activator of Rac, to inhibit chemotaxis and promote T cell activation by Nef, while activation of the Pak2 kinase and a GTPase exchange factor such as Vav induces cytoskeletal rearrangements and downstream effector functions (*7*, *8*). The polycomb protein Eed was found to interact with the N-terminus of Nef to assemble another kinase-containing complex that includes the tyrosine kinase Lck (*9*). Transport processes mediated by Nef include the interference with intracellular trafficking pathways to downregulate CD4 from the cell surface. This interaction was linked to endocytic AP clathrin adaptor complexes; however, while the precise

† This work was supported by a grant from the Deutsche Forschungsgemeinschaft to M.G. (GE-976/1).

* To whom correspondence should be addressed. Phone: +49 231 133-2366. Fax: +49 231 133-2399. E-mail: matthias.geyer@mpi-dortmund.mpg.de.

‡ Max-Planck-Institut für Molekulare Physiologie.

§ Present address: K. U. Leuven, Afd. Fotochemie & Spectroscopie, Celestijnenlaan 200F, B-3001 Heverlee, Belgium.

|| Medizinische Hochschule Hannover.

[1] Abbreviations: FCS, fluorescence correlation spectroscopy; GST, glutathione *S*-transferase; HIV, human immunodeficiency virus; IPTG, isopropyl β-D-thiogalactopyranoside; MPE, multiphoton excitation; Nef, protein product encoded at the 3′ end of the HIV/SIV genome; NMT, *N*-myristoyltransferase; PMSF, phenylmethanesulfonyl fluoride.

10.1021/bi052052c CCC: $33.50
Published on Web 01/31/2006

subunits are still a matter of debate, recent findings suggested that both internalization and intracellular retention mechanisms are involved (*10*−*13*).

Virtually all biological activities of Nef require its N-terminal myristoylation for the association with cellular membranes (*5*, *14*). Myristoylated proteins start with the sequence Met-Gly, but the initiating methionine is removed during translation and myristate is amide linked to the glycine (*15*). Thus, because of its functional importance the myristoylation signal MGxxxS(K/R) is found to be totally conserved in all Nef alleles from different subtypes and stages of disease (*16*). However, cellular fractionation assays from transient transfections showed that less than 60% of all Nef is localized at membranes while the remaining portion is found to be cytosolic (*17*−*20*). Myristoylation (C14) is indeed the shortest of all fatty groups and suggested to be the weakest stable modification for membrane association (*15*).

The 24−29 kDa HIV-1 Nef protein adopts a two-domain structure encompassing a flexible membrane anchor domain (residues 2−61 in Nef_{SF2}) and a folded core domain (residues 62−210). The core domain again contains a C-terminal flexible loop of 33 residues (152−184) that is thought to mediate trafficking interactions (*5*). Protein structures of Nef have been determined for the core domain by NMR spectroscopy and X-ray crystallography (*21*−*23*) and for the flexible anchor domain by NMR (*24*), but not yet for the full-length protein due to the low stability and solubility and the high degree of intrinsic flexibility. The amino acid numbering used in the remainder corresponds to the Nef-SF2 allele which contains an insert of four additional residues (positions 23−26) in the N-terminal variable duplication region relative to the NL4-3 or LAI Nef sequences.

N-Myristoylation is typically a "permanent" modification; the half-life of the acyl chain moiety is equivalent to that of the polypeptide backbone (*1*, *15*). The transition from a membrane-bound to a cytosolic form of Nef might thus be accompanied by conformational changes within the protein that expose or hide the fatty acid moiety and additionally influence the structure of the anchor domain. We therefore intended to study differences in the myristoylated and nonmyristoylated form of Nef by biochemical means. The conformation and dynamics of the myristoylated protein in aqueous solution may thereby reflect the cytosolic form of Nef while the unmodified protein rather corresponds to the membrane-bound state when the myristate is inserted into the lipid bilayer. We first established an N-myristoylation assay in *Escherichia coli* cells by coexpression of Nef with the *N*-myristoyltransferase and the use of a codon-optimized Nef plasmid that significantly increased the yield of modified protein. We then applied size exclusion chromatography, fluorescence correlation spectroscopy, and western blot analysis of the protein samples, which indicated a smaller size and a shorter diffusion time for the myristoylated Nef protein, as well as different antibody recognition and proteolytic digestion patterns. Finally, analytical ultracentrifugation revealed that myristoylated Nef prevails in a monomeric state while the unmodified form existed in an equilibrium of monomer, dimer, and trimer assemblies. These data suggested conformational changes within Nef that may reflect the reversible transition from a membrane-bound to a cytosolic form.

EXPERIMENTAL PROCEDURES

Synthesis of the Codon-Optimized nef Gene. The analysis of the codon usage distribution in the HIV-1 nef_{SF2} gene (accession number K02007) for expression in *E. coli* bacterial cells was performed with the help of the graphical codon usage analyzer (http://gcua.schoedl.de/). The wild-type Nef_{SF2} plasmid was a kind gift from Matija Peterlin at UCSF (*11*). Four regions were identified where AGG, AGA, and CTA codons accumulated, that together covered 10 out of 13 rare codons. Following the mega primer method for site-directed mutagenesis, sense and antisense oligonucleotides of 31−36-mer length were designed that included the silent mutations to more commonly used codons. In a first round of PCR, five oligonucleotide fragments including the 5′ and 3′ start and stop primers were amplified on the wild-type gene template. The resulting fragments from 72 to 283 nucleotide length were purified on 2.5% agarose gel electrophoresis with the QIAquick gel extraction kit (Qiagen) and eluted with 40 μL of water. In a second round of PCR, 2 μL from each of the five fragments was mixed together and amplified with the expand high-fidelity PCR system (Roche) for three cycles (94, 50, and 72 °C) before addition of the initiating start and stop primer. The resulting full-length *nef* gene was cut with *Nco*I and *Eco*RI restriction enzymes and ligated into the pProEx-HTa vector (Stratagene) for bacterial expression. Four positive clones of the obtained Nef plasmid were sequenced, out of which one showed the correct codon-optimized sequence.

Protein Expression, Myristoylation, and Purification. For the development of a myristoylated Nef expression system in *E. coli* the codon-optimized *nef* gene was amplified by PCR with *Nco*I and *Hin*dIII restriction sites at the 5′ and 3′ ends, respectively, and omitted for a stop codon at the 3′ end. This fragment was cloned into the pET-23d expression vector (Novagene) that contained an ampicillin resistance and a C-terminal His_6 tag for affinity chromatography. Therefore, upon expression of Nef residues KLAAALEHHHHHH were attached at the C-terminus to the protein product. The plasmid DNA of the human *N*-myristoyltransferase (NMT, accession number NP_066565) was a kind gift from Jeff Gordon (pBB218; ref *25*). A fragment that codes for an N-terminally truncated NMT (residues 81−496) and misses the ribosomal binding unit was amplified with *Nde*I and *Eco*RI restriction sites and cloned in the pET-30a expression vector (Novagene) that carries a kanamycin resistance.

Both plasmids were cotransformed in BL21(DE3) cells and maintained with double antibiotic selection. For protein production, a fresh colony was picked, expressed first at 37 °C before reduction to 28 °C, and induced at an OD_{600} of 0.8−1.2 with 0.5 mM IPTG for 5 h growth. About 10 min before induction myristic acid was supplemented as the cosubstrate to the cells. For each liter of cell culture, 10 mL from a solution of 0.6 mM BSA (fraction V; Sigma) and 5 mM myristic acid (Sigma) was added, which was dissolved prior to application at pH 9 (NaOH) and 50 °C. Cells were fluidized in lysis buffer A (20 mM Tris-HCl, pH 8.0, 500 mM NaCl, 5 mM β-mercaptoethanol, 1 mM PMSF) with 25 mM imidazole and cleared by spinning for 45 min at 30000*g*. The lysate was loaded onto 5 mL of Ni-NTA resin (Qiagen) that had been preequilibrated with lysis buffer

(without PMSF). After being washed with 10 volumes of lysis buffer A the protein was eluted with 10 volumes of lysis buffer A using a linear gradient from 25 to 250 mM imidazole. The protein-containing flow-through was concentrated and further purified by gel filtration on a Superdex 75 column (16/60, column volume 120 mL; Amersham) in 20 mM Tris-HCl (pH 8) and 50 mM NaCl. Fractions were analyzed by SDS−PAGE, and fractions containing myristoylated Nef (about 96% pure) were concentrated and stored at −80 °C. For NMR experiments and analytical gel filtration the protein was dialyzed against 20 mM KP_i buffer and 50 mM NaCl as indicated. Protein concentrations were determined by extinction coefficient measurements.

For direct comparisons a nonmyristoylated Nef variant (G2A) was cloned similarly in the pET-23d vector and expressed without the NMT. Two other truncated forms, Nef(45−210) and Nef(59−210), were cloned in the pProEx-HTa vector with *Nco*I and *Eco*RI restriction sites, expressed, and purified as before, and the hexahistidine tag was cleaved off at 4 °C over 12 h with Tev protease. Nef proteins were depleted of uncleaved His-Nef and of the protease by affinity chromatography and gel filtration.

Mass Spectrometry, NMR Spectroscopy, and Western Blot Analysis. Analytical mass spectrometry was performed in house using MALDI-TOF and ESI methods. Proton NMR spectroscopy was performed with a Varian Inova 600 MHz spectrometer at 27 °C with concentrations of 0.2−0.4 mM Nef protein in 20 mM KP_i buffer at pH 7.6. Western blot analysis was run on 15% SDS gel electrophoresis with 2 or 8 μg of Nef subjected to each lane, respectively. The monoclonal anti-Nef antibody was a kind gift from Mark Harris, University of Leeds, and was used in a 1:2500 dilution. The anti-His antibody was purchased from Santa Cruz Biotechnology (1:2000); the peroxidase conjugated anti-mouse antibody was used in a 1:4000 dilution (all in PBS with 0.05% Tween).

Analytical Gel Filtration. Analytical gel filtration was performed with a multicomponent Waters 626 LC system (Waters, MA) using either a Superdex 75 column (10/300, column volume 25.7 mL), a Superdex 200 column (10/300, 24.5 mL; both from Amersham), or a Biosep-SEC-S2000 column (300 × 1.8 mm; Phenomenex). The columns were equilibrated with 20 mM KP_i buffer (pH 7.8), 50 mM NaCl, and 2 mM DTE, respectively, following injection of the protein samples. The flow rate was set to 0.5 mL/min. Elution profiles were monitored by UV absorption at 280 nm. The void volume (V_0) was determined with blue dextran (Sigma). The columns were calibrated with the following standards (Amersham): albumin (67 kDa), ovalbumin (43 kDa), chymotrypsinogen A (25 kDa), and ribonuclease A (13.7 kDa). The ratio of elution volume to void volume (V_e/V_0) was plotted versus the log(MW) for each standard to generate a linear calibration curve. Myristoylated or mutant Nef was dialyzed from frozen stocks into the equilibration buffer, diluted to a concentration of 1 mg/mL each, and injected onto the column at a volume of 90 μL. The apparent MW of each Nef protein was determined from the standard curve. Gel filtration experiments were performed repeated times at room temperature.

Analytical Centrifugation and Sedimentation Velocity Experiments. All experiments were done with a Beckman/Coulter XLA analytical ultracentrifuge equipped with UV scanner optics using the eight-hole An-Ti analytical rotor. Sedimentation velocity experiments were done in double sector centerpieces made of charcoal-filled epon at a speed of 50000 rpm and 20 °C. Samples were scanned at 280 nm. The sedimenting boundary was analyzed using the program SEDFIT (*26*). This program uses a set of numerical solutions of Lamm's differential equation and calculates by regularization a differential sedimentation coefficient distribution corrected for diffusional broadening. The sedimentation coefficient distributions were corrected for buffer viscosity and density using a partial specific volume of 7.291×10^{-4} $m^3\ kg^{-1}$ for nonmyristoylated and myristoylated Nef (neglecting the contribution of the myristoyl moiety).

Fluorescence Correlation Spectroscopy Setup and Fitting Procedure. Fluorescence emission spectra were carried out using a FluoroMax-3 spectrofluorometer (SPEX Instruments, Edison, NJ) at an excitation wavelength of 280 nm and a band-pass of ±1 nm as described (*27*). Fluorescence emission was monitored with a band-pass of ±2.5 nm between 300 and 500 nm.

For combined fluorescence correlation spectroscopy (FCS) and confocal laser scanning microscopy (CLSM), we extended our MRC-1024 (Bio-Rad) coupled via a side port to an inverted microscope (Nikon, Eclipse TE-300 DV, infinity corrected optics, additionally equipped with a triple chroic mirror) enabling fluorescence excitation in a nonscanning mode in the focal plane of the objective lens (60× water immersion objective, NA 1.2, collarrim correction). In case of FCS measurements the collected fluorescence is transmitted to an optical module at the bottom exit of the microscope, which is connected via fiber optics (core diameter 25 μm, serving as a pinhole) to a highly sensitive photodetector [single photon counting avalanche diode (SPAD)]. The output signal of this SPAD is directly fed into a hardware correlator card (ALV-5000/E multiple tau digital correlator; ALV-Laser GmbH, Langen) designed as a single board unit for IBM-compatible computers. The ALV digital correlator generates the real-time autocorrelation function or even cross-correlation functions (if two input signals are provided) with a fixed range of simultaneous lag times between 200 ns and several hours. The measurements were conducted at 25 °C.

The autocorrelation curves were fitted by the nonlinear function:

$$y = [1 - \mathrm{P1} + \mathrm{P1}\exp[(-x)/\mathrm{P2}][1/(\mathrm{P3}(1 + x/\mathrm{P4}))] \times [1/(1 + \mathrm{P5}(x/\mathrm{P4}))\wedge 0.5]] + \mathrm{P6}$$

(assuming a single species) with the following parameters: P1 = triplet fraction; P2 = triplet relaxation time; P3 = $N = 1/G_0$ (number of molecules); P4 = average residence time; P5 = $(\omega_0/z)\wedge 2$ with ω_0, z structural parameters of the ellipsoidal measuring volume; and P6 = offset. The diffusion time τ_{diff}, i.e., the average lateral transit time of the particles through the focus, relates to the diffusion coefficient D by $D = \omega_0^2/4\tau_{diff}$. For approximately spherical particles, the hydrodynamic radius r_h of the particle can be obtained from the diffusion coefficient via the Stokes−Einstein equation $D = kT/(6\pi\eta_V r_h)$, where T is the temperature, k the Boltzmann's constant, and η_V the local viscosity. Measurement data were analyzed with Origin 7.0 (OriginLab Corp.).

RESULTS

Codon Optimization of the nef Gene Significantly Increased Protein Expression Levels. The difference of codon usages between various organisms is often known to influence expression levels at the stage of protein translation (*28*). This results, e.g., in difficulties to express large amounts of eukaryotic or viral proteins in prokaryotic cells, such as *E. coli*. Also, it may imbalance the expression levels of two binding proteins or multiple subunit complexes when coexpressing them simultaneously from different strains. To increase the production of the HIV-1 Nef protein, allele SF2, in *E. coli* cells and to further establish a coexpressing system for myristoylation, we analyzed the coding sequence for the three most rarely occurring codons, AGG, AGA, and CTA. These codons account for 2% and 4% of all translated arginines and 4% of all leucines, respectively, in the *E. coli* K12 genome. Assuming that every tenth amino acid is an arginine or leucine, respectively, these codons naturally occur only once among 500 or 250 codons, respectively. The HIV-1 SF2 *nef* gene contains two AGG, seven AGA, and four CTA codons within the 210-residue protein, accumulating partly in an arginine-rich cluster from positions R17 to R21 and at positions R109 and R110. Thus, we synthesized a codon-optimized *nef* gene in which 10 out of 13 rare codons were replaced by silent mutations using a cloning strategy based on five overlapping oligonucleotide fragments (Figure 1A). Only one AGA and two CTA codons remained that were spread over the full nucleotide sequence. Upon design of the optimized *nef* gene we analyzed possible RNA secondary structures of the corresponding mRNA in order to avoid highly stable RNA structures which might affect translation in the *E. coli* system.

For initial expression tests of the unmodified protein, we cloned the wild-type and the codon-optimized *nef* genes into a T7-based prokaryotic expression vector with an N-terminal His_6 tag and transformed the plasmids into *E. coli* BL21-(DE3) cells. Additionally, we transformed the wild-type plasmid into BL21-CodonPlus(DE3)-RIL cells (Stratagene) that carry extra copies of the *argU*, *ileY*, and *leuW* tRNA genes. The tRNAs encoded by these genes recognize the AGA/AGG, AUA, and CUA mRNA codons, respectively. The protein overexpression of these three expression systems after induction with IPTG is compared in Figure 1B. Indeed, the CodonPlus-RIL cells and the codon-optimized Nef plasmid yielded significantly higher expression levels at 1, 2, and 4 h after induction than the wild-type gene. Expression of the rare tRNAs in the CodonPlus-RIL cells required chloramphenicol as the selection marker, which led to expression of the 25 kDa chloramphenicol acetyltransferase as can be seen on SDS−PAGE. On average, from 1 L of medium culture we obtained about 6 mg of purified Nef protein using the wild-type plasmid, 60 mg using the CodonPlus inducible system, and 100 mg using our codon-optimized *nef* plasmid. Thus, codon optimization of HIV-1 SF2 Nef for the *E. coli* system proved to significantly increase the prokaryotic protein expression levels.

Nef Is Effectively Myristoylated by Coexpression with the N-Myristoyltransferase. We next intended to produce myristoylated Nef in bacterial cells by coexpression of the *N*-myristoyltransferase (NMT) and addition of myristic acid as substrate. To this end we cloned the human NMT in a

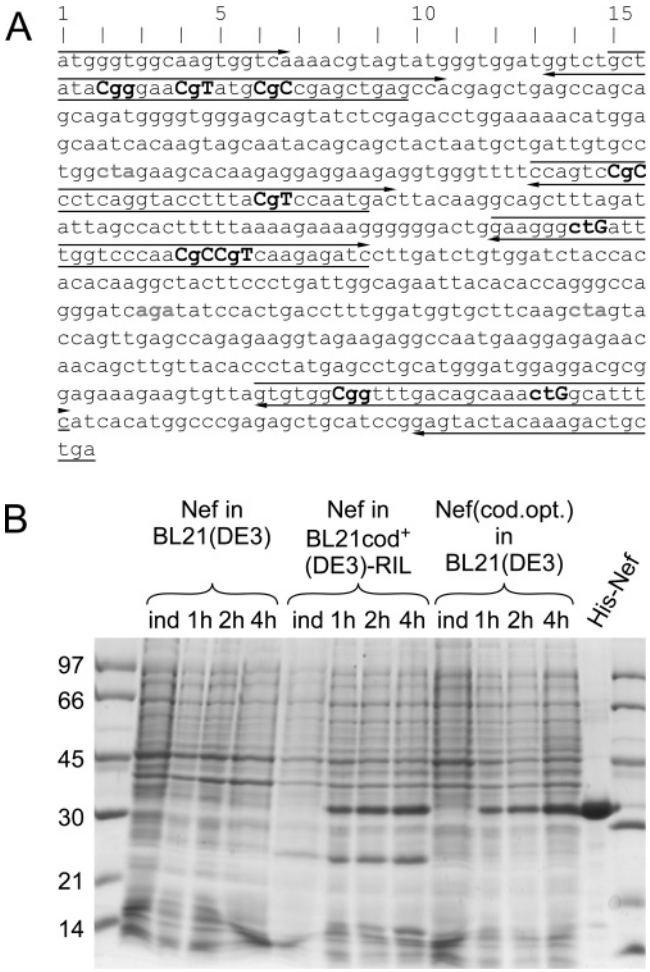

FIGURE 1: Codon optimization of HIV-1 Nef_{SF2} for *E. coli* bacterial cells resulted in significantly higher protein expression levels. (A) cDNA of the codon-optimized Nef gene. AGA, AGG, and CTA codons that were modified are indicated in bold; changed nucleotides are in capital letters. The sense and antisense oligonucleotide sequences used for PCR amplification are indicated by arrows. (B) SDS−PAGE analysis of Nef protein expression in *E. coli* cells. Displayed is each time 10% of the 1 mL cell lysate from three different expression tests was taken before induction and 1, 2, and 4 h after induction, respectively. Wild-type Nef from the pProEx-HTa expression vector was first expressed in BL21(DE3) cells and next in BL21-CodonPlus(DE3)-RIL cells containing a chloramphenicol resistance for rare tRNA expression, and finally the codon-optimized Nef plasmid was expressed again in BL21(DE3) cells. The purified Nef protein including the N-terminal His_6 tag is shown to the right. Proteins were stained with Coomassie blue.

T7-based expression vector carrying a kanamycin resistance. In this plasmid the N-terminal ribosomal binding unit (1−80) was cleaved off for better solubility and enzymatic activity and in order not to overload the ribosomes in the prokaryotic *E. coli* expression system. The codon-optimized *nef* gene was cloned in the pET-23d expression vector using the initiating methionine within the *Nco*I restriction site as start codon and a C-terminally attached His_6 tag for affinity purification. Both the codon-optimized Nef plasmid and the human NMT plasmid were cotransformed in BL21(DE3) cells and maintained by ampicillin and kanamycin selection during expression. Shortly before induction with IPTG the fatty acid was delivered from a highly concentrated myristic acid−BSA solution. We tested four different expression temperatures from 18 to 37 °C and found an expression of 5 h at 28 °C to yield the highest protein levels and lowest

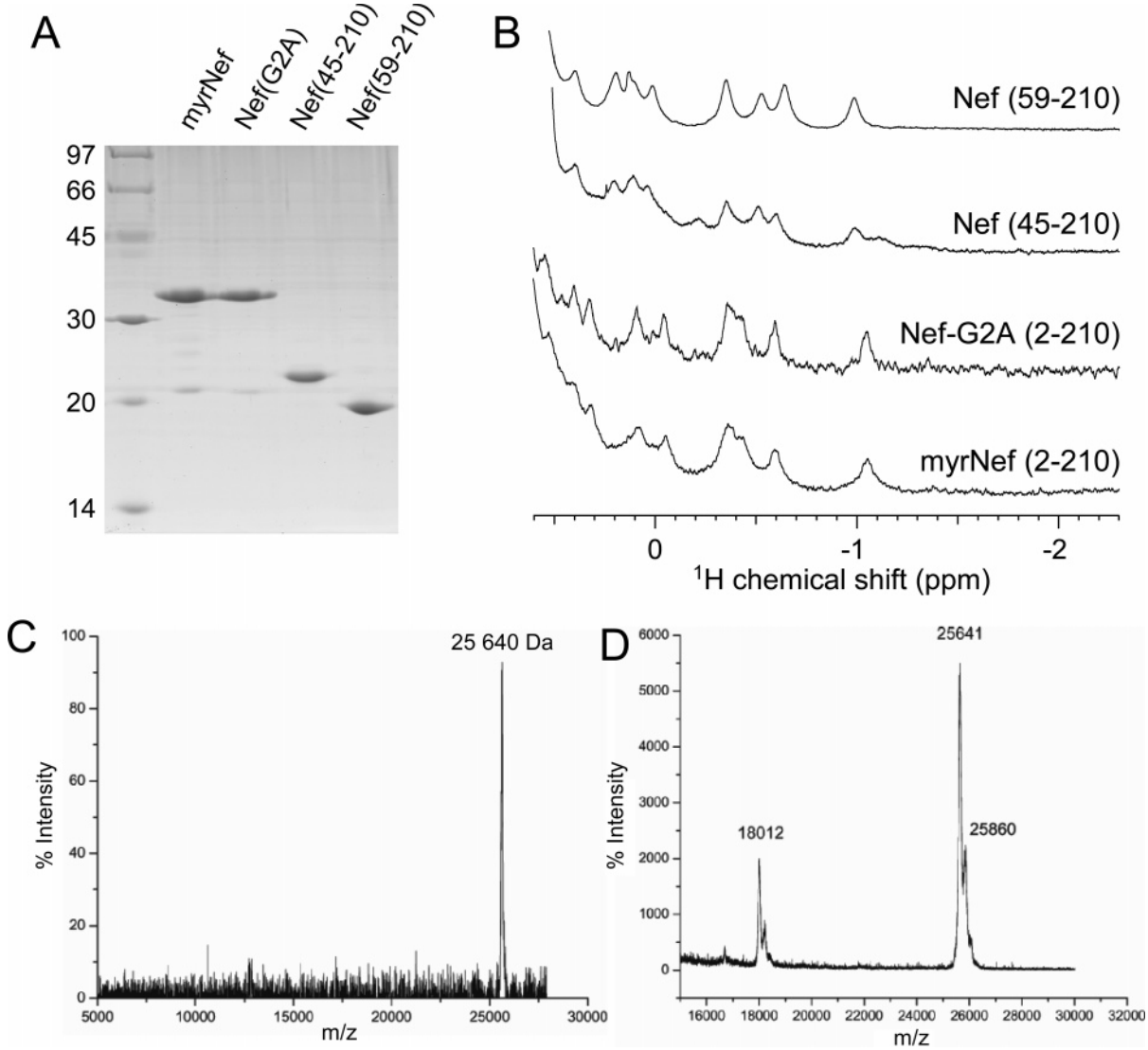

FIGURE 2: Purification and analytical investigations of myristoylated and nonmyristoylated Nef proteins. (A) SDS−PAGE display of purified Nef protein fragments used in this study. Proteins were stained with Coomassie blue. (B) Proton NMR spectra confirmed the folding of the various Nef proteins used. Shown is the high-field-shifted region of the spectra that typically displays resonances of methyl groups in close contact with aromatic side chains as found in the Nef core domain structure. (C) ESI mass spectrometry analysis of the myristoylated wild-type Nef protein attached with a C-terminal His_6 tag. The measured protein mass of 25640 Da exactly matches the calculated mass. (D) MALDI-TOF mass spectrometry analysis of a myristoylated Nef protein sample purified at room temperature. The degradation product at 18.0 kDa resulted from proteolytic digestion of the N-terminal anchor domain and corresponded to the stable core domain of SF-2 Nef (70−210). Note that both mass spectra did not exhibit any nonmyristoylated protein fraction.

degree of degradation of myristoylated Nef. The lipidated protein was found in the soluble fraction of the cell lysate, and protein purification was subsequently performed using standard protocols with nickel affinity chromatography. On average, 1 L of expression medium yielded about 30 mg of purified myristoylated Nef protein while the nonoptimized plasmid yielded only 2 mg of lipidated protein.

For further biochemical investigations wild-type myristoylated Nef, a myristoylation-defective full-length Nef (G2A), and two N-terminally truncated forms, (45−210) and (59−210), respectively, were expressed and purified. The Coomassie-stained purified proteins are displayed on 15% SDS−PAGE in Figure 2A. Both full-length proteins showed a truncation at 22 kDa that corresponded to less than 5% of the total protein yield. The myristoylated Nef protein runs at a similar size to the unmodified form, while some myristoylated proteins such as Arf1 appeared slightly smaller than their nonlipidated forms (*29*). MALDI-TOF and ESI mass spectrometry confirmed a single mass of 25640 Da for the wild-type myristoylated Nef protein that most accurately reflects the calculated mass of 25640 Da (Figure 2C,D). The MALDI-TOF spectrum that was recorded of a protein purified at room temperature additionally identified a mass at 18012 Da, corresponding to the truncated Nef fragment (Figure 2D). This fragment represented the stable core domain of Nef from position V70 to the C-terminus including the noncleavable His_6 tag, as was reported similarly in early limited proteolytic digestion experiments for the NL4-3 Nef protein (*30*). The MALDI-TOF spectrum additionally showed a second peak of 25860 Da mass that might result from a bound myristoyl group (228.4 Da) to Nef. Since a similar pattern was also found for the truncated Nef protein (70−210), the binding site might be located on the Nef core domain structure. Importantly, both mass spectra did not show any nonmyristoylated full-length protein, indicating the full modification of all Nef protein.

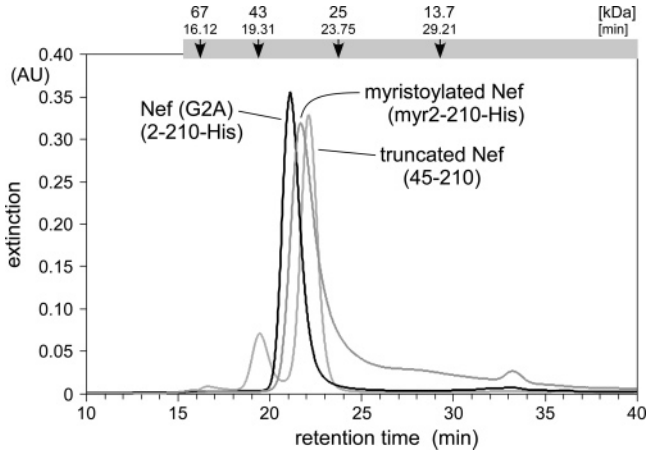

FIGURE 3: Analytical gel filtration of Nef proteins suggested a myristoylation-dependent conformational change. Elution profiles of myristoylated Nef (myr2−210), nonmyristoylated Nef (2−210, G2A), and N-terminally truncated Nef (45−210) are shown. Both full-length proteins carried a C-terminal His tag of 10 residues. Measurements were performed on a Superdex 75 (10/30) column with an elution volume of 0.5 mL/min in 20 mM KP_i buffer (pH 7.6) and 50 mM NaCl. Molecular masses (kDa) and retention times (min) of marker proteins are shown on top. The myristoylated Nef protein eluted at a retention time later than the nonmyristoylated form, suggesting a smaller globular size. The truncated Nef (45−210) appeared still smaller than the myristoylated full-length protein and showed some dimeric and multimeric fractions.

We next analyzed the solubility and folding of the Nef protein constructs with proton NMR spectroscopy (Figure 2B). One-dimensional spectra of protein samples concentrated to 0.2−0.4 mM in 20 mM KP_i aqueous buffer (pH 7.6) and 50 mM NaCl were measured at 27 °C, accumulating 256−1024 scans each. A section showing the high-field-shifted regions from 0.6 to −2.3 ppm is displayed for myristoylated Nef, the nonmyristoylated form G2A, and the two truncations (45−210 and 59−210). The resonance signals observed in this region are expected to correspond to methyl groups that are in close contact to aromatic side chain residues, being therefore an indication for the folding of the hydrophobic core domain. The dispersion of the resonance lines indicated that all four protein constructs were similarly well folded. However, the broadened line shape of the myristoylated Nef indicated a higher tendency for aggregation compared to the truncated forms. Interestingly, also minor differences as, e.g., the shift of the peak at −0.42 ppm in the full-length protein to −0.55 ppm in the truncated proteins can be observed, suggesting small changes in the chemical environment of this residue.

Analytical Gel Filtration Revealed a Smaller Size of Myristoylated Nef Compared to the Nonmyristoylated Protein. The molecular dispersion of the lipidated Nef protein in comparison to the nonmodified forms was next studied by size exclusion chromatography. Three different analytical gel filtration columns with variable elution profiles were used, and experiments were run several times using different buffer solutions and temperatures. To our surprise, the myristoylated full-length protein always eluted at a retention time later than the unmodified G2A mutant (Figure 3). On a Superdex 75 column equilibrated in low salt phosphate buffer the full-length Nef(G2A) protein eluted fastest at 21.07 min (at a flow rate of 0.5 mL/min), corresponding to a calculated globular size with an apparent mass of 35.7 kDa. The elution profile was well defined by a single symmetrical absorption line. Migration of myristoylated Nef followed at 21.64 min, which is significantly different from the nonlipidated form. Interestingly, also the shape of the elution profile became asymmetric and showed tailing toward higher retention times. The peak of the elution profile corresponded to a globular protein size with a calculated mass of 33.3 kDa. The N-terminally truncated Nef protein (45−210) appeared again later than the myristoylated full-length protein at a retention time of 22.07 min or an apparent mass of 31.6 kDa. The difference in size to the unmodified full-length Nef-(G2A) mutant of 4 kDa reflected approximately the mass of the N-terminal truncation ($MW_{(2-44)}$: 4.7 kDa). Of note, other than the two full-length proteins the truncated form always exhibited two fractions of higher molecular weight that could correspond to dimeric and multimeric formations. In conclusion, we find that the myristoylated Nef protein of slightly higher mass appeared significantly smaller by size exclusion chromatography than the nonmyristoylated form, suggesting a more compact conformation for the lipidated protein.

Western Blot Analysis Showed Myristoylation-Dependent Differences in the Recognition and Degradation of Nef. Conformational changes in protein isoforms often correlate with different proteolysis patterns and modified recognition profiles of primary antibodies. We therefore intended to prove the indication of myristoylation-dependent different sizes of Nef by western blot analysis. To this end, two antibodies were used, one directed against an epitope in the very N-terminal region of Nef and a second one directed against the C-terminal His tag. The N-terminal monoclonal anti-Nef antibody was a kind gift from Mark Harris, University of Leeds. The western blot analyses of myristoylated (myr) and nonmyristoylated Nef proteins (G2A) are shown side-by-side on 15% SDS−PAGE, each loaded with 8 μg of purified protein (Figure 4). First, Coomassie staining displayed the protein input used including the C-terminal His_6 tag and confirmed two bands of similar intensities that migrated at 34 kDa (Figure 4A). Next, the anti-Nef antibody was used. Indeed, while the nonmyristoylated Nef protein was properly recognized, the detection of myristoylated Nef was considerably reduced, suggesting different conformations of the two migrating proteins (Figure 4B). The targeting of the antibody against the very N-terminal epitope in the anchor domain of Nef is confirmed by the observation that only full-length Nef is detected in both lanes but not any N-terminal truncations. Next, the anti-His antibody that recognized the C-terminal epitope revealed differences in the proteolytic digestion pattern of both proteins (Figure 4C). After purification the proteins were kept at room temperature for approximately 6 h before subjection to SDS−PAGE analysis. Both proteins showed truncations that migrated at 23 kDa and corresponded to the Nef core domain from position 70 to position 210 as described before (*30*). However, the intermediate proteolysis fragments observed between 34 and 23 kDa indicate different cleavage patterns within the N-terminal anchor domain. Moreover, another small fragment at 11 kDa that corresponded most likely to truncations in the C-terminal flexible loop of Nef is only observed in the myristoylated form but not in the nonlipidated protein. Finally, we applied limited enzymatic proteolysis with myristoylated and nonmyristoylated Nef protein (Figure 4D). To this end, we used 70 μg of Nef at a concentration

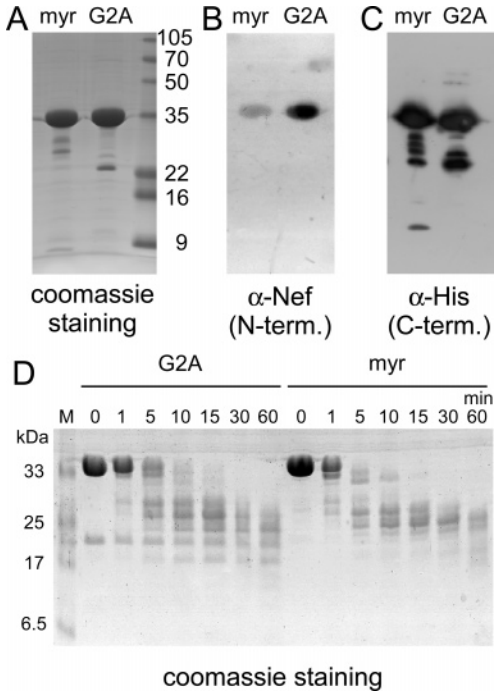

FIGURE 4: Western blot analysis exhibited myristoylation-dependent differences in the accessibility and proteolysis of Nef. The migration of myristoylated (myr) and nonmyristoylated (G2A) Nef proteins is shown on 15% SDS−PAGE analysis, respectively. 8 μg of purified proteins was subjected to each lane. (A) Coomassie staining of the two protein forms used. (B) Differences in the recognition of Nef using an anti-Nef antibody directed against an N-terminal epitope. While the nonmyristoylated Nef was properly recognized by the antibody, the detection of the myristoylated Nef was considerably reduced. Note that only the full-length protein is detected in both lanes but not any truncations of Nef, confirming the very N-terminal epitope targeting of the antibody. (C) Differences in the proteolytic digestion pattern of myristoylated and nonmyristoylated Nef. The truncations of Nef that occur in the cell lysate and during protein purification are detected by an anti-His_6 antibody that recognized the C-terminal epitope. (D) Time course of an enzymatic proteolysis experiment of unmodified Nef(G2A) and myristoylated Nef. The proteolytic digest using Nef with elastase and trypsin in a 500:1 ratio (w/w) was followed over 60 min. Each lane contained 3 μg of Nef subjected to 18% SDS−PAGE and stained with Coomassie blue.

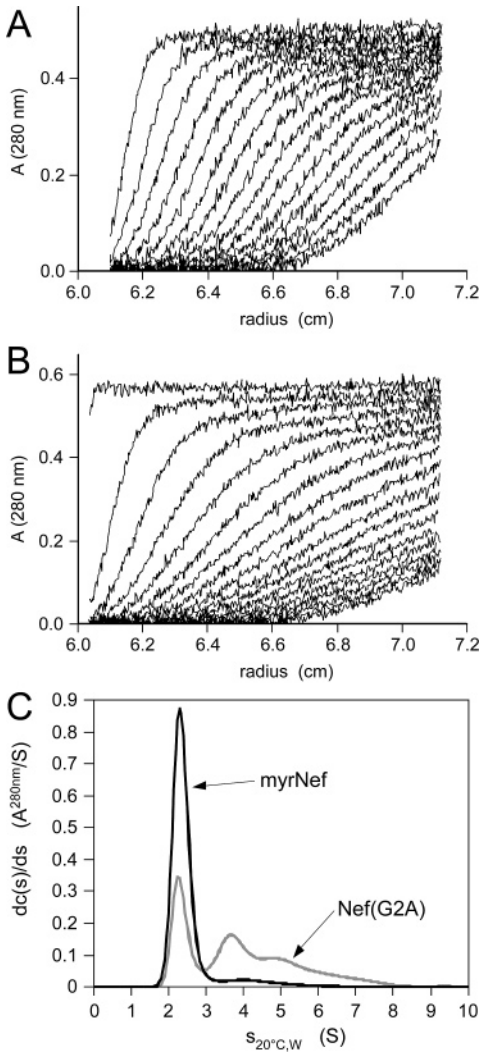

FIGURE 5: Analytical ultracentrifugation of myristoylated and nonmyristoylated HIV-1 Nef. (A) Sedimentation curves of 9 μM myristoylated Nef in an analytical ultracentrifuge at 50000 rpm in 20 mM Tris-HCl buffer (pH 8.0). Scans were taken every 11 min, and every second scan is depicted. (B) Sedimentation curves of 9 μM nonmyristoylated Nef(G2A), recorded as in (A). (C) Differential sedimentation coefficient distributions for myristoylated and nonmyristoylated Nef(G2A) calculated from the above sedimentation traces using the SEDFIT program (*26*). While the unmodified form of Nef existed in an oligomeric equilibrium of monomer, dimer, and trimer fractions at 2.3, 3.7, and 5.1 S, the myristoylated Nef prevails in a monomeric state at 2.3 S.

of 2 mg/mL and added both elastase and trypsin in a 1:500 ratio from a 0.1 mg/mL stock solution. The digest was followed over 60 min with each 3 μg sample taken at defined time points and subjected to SDS−PAGE analysis. Small but distinct differences of the degradation could be observed, e.g., by a fragment at 18 kDa that appeared after 5 min in Nef(G2A) but not in myristoylated Nef. Moreover, the kinetics of truncations resulting in fragments from 30 to 25 kDa size appeared differently. Together, these data again suggested different accessibilities of the two protein forms resulting from conformational changes upon myristoylation.

Analytical Ultracentrifugation Showed Myristoylation To Shift the Oligomeric Assemblies of Nef toward a Monomeric Form. To further test the implications of myristoylation on the oligomerization state of Nef, we performed sedimentation velocity analysis using analytical ultracentrifugation experiments (Figure 5). The sedimentation traces of a 9 μM concentrated protein sample of myristoylated or nonmyristoylated Nef were measured at 50000 rpm in 20 mM Tris-HCl buffer at pH 8.0 and 20 °C (Figure 5A,B). The differential sedimentation coefficient distributions showed for nonmyristoylated Nef a sedimentation behavior corresponding to a mixture of three species sedimenting with 2.3, 3.7, and 5.1 S (Svedberg), respectively (Figure 5C). These three species most likely indicated self-association of Nef that may correspond to monomeric, dimeric, and trimeric forms. Indications of dimer and trimer Nef accumulations have been indeed identified before in protein crystals with different packing units (*23*). In contrast to this, the myristoylated Nef sample showed a prominent component sedimenting with 2.3 S and only a minor impurity of less than 8% at 4 S. This observation suggested that myristoylation of Nef resulted in monomerization in aqueous solution, meaning that the cytosolic form of Nef is rather monomer while the membrane-bound form might occur in an multimeric equilibrium. From 2.3 S and 25.4 kg molar mass a

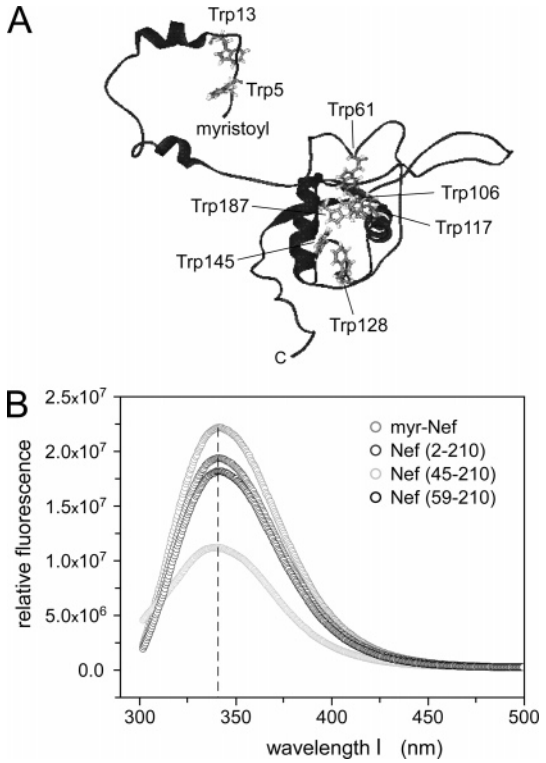

FIGURE 6: Fluorescence emission spectra of myristoylated, nonmyristoylated, and N-terminally truncated HIV-1 Nef proteins. (A) Nef_{SF2} contains eight tryptophans in its structure. Five of these form the core domain structure, out of which four are highly conserved while three are located in the N-terminus. Displayed is a full-length model of Nef that is assembled from individual structures of the anchor (1−61) and core (62−210) domain. PDB accession numbers are 1QA5 (*24*) and 2NEF (*21*), respectively. (B) Fluorescence emission spectra of various Nef protein fragments. The excitation wavelength was set to 280 nm with ±1 nm slits. The emission wavelength was recorded from 300 to 500 nm, integrated in steps of 1 nm with a 1 s integration time and ±5 nm slits. Spectra were recorded at 20 °C in 20 mM Tris-HCl (pH 7.6), 50 mM NaCl, and 5 μM protein concentration.

frictional coefficient of 1.37 is calculated (*26*), indicating the molecule to have an elongated structure or a globular structure with some protrusion contributing to the larger friction.

Fluorescence Correlation Spectroscopy Revealed Different Diffusion Times. To obtain more information on the influence of the myristoylation on the conformation and dynamics of Nef, we performed fluorescence studies in solution. First, fluorescence emission spectra were recorded by excitation of the intrinsic tryptophans within Nef at 280 nm. Nef-SF2 contains a high number of eight tryptophans, the anchor domain possesses three highly conserved tryptophans (positions 5, 13, 61) while the core domain is formed by five tryptophans, out of which four (positions 117, 128, 145, 187) are highly conserved and almost completely hidden within the structure. The location of the typtophan residues is displayed in a model structure (*16*) of full-length Nef (Figure 6A). Fluorescence emission spectra revealed that the fluorescence maximum at 341 nm and the natural line width are similar for myristoylated Nef, the nonmyristoylated Nef(G2A), and the N-terminally truncated proteins Nef(45−210) and Nef(59−210) (Figure 6B). Since the reciprocal value of the line width is related to the time of the fluorescence decay, we conclude that the local environments around the excited states S_1 are similar for the tryptophan moieties in both lipidated and nonlipidated Nef.

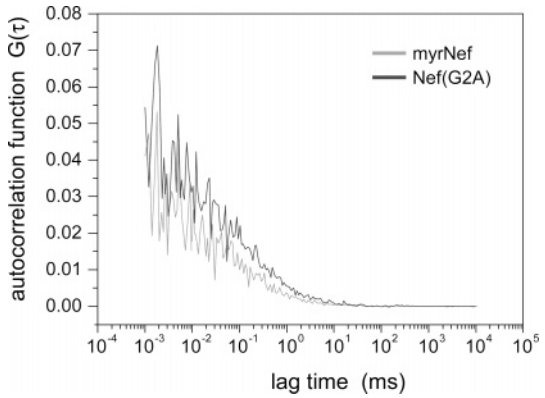

FIGURE 7: Fluorescence autocorrelation spectra of myristoylated and nonmyristoylated Nef showed different diffusion times. Fluorescence correlation spectra were recorded using direct three photon excitation of the tryptophans at 840 nm. The measurements were performed at an average laser power of 120 mW using a titanium sapphire laser (coherent) with high repetition rate (76 MHz) and short pulse width (~200 fs). Protein concentrations of 38 μM in aqueous solutions were used, and spectra were recorded at 25 °C.

Table 1: Characteristic Translational Diffusion Times of Myristoylated and Nonmyristoylated HIV-1 Nef Proteins

molecule	diffusion time (τ_{diff}) (ms)
$myrNef_{SF2}$ (myr2−210)	0.08 ± 0.023
Nef_{SF2} (G2A, 2−210)	0.15 ± 0.017
Nef_{SF2} (45−210)	0.12 ± 0.025
Nef_{SF2} (59−210)	0.13 ± 0.019

Next, we tested the existence of multiphoton excitation within Nef using a home-build fluorescence correlation microscope equipped with a mode-locked Ti-Sa laser that allows for excitation between 700 and 1000 nm (*31*). To this end, we excited the Nef protein with a wavelength of 840 nm, which is three times longer than its one photon absorption maximum at 280 nm. To our surprise, we indeed observed fluorescence correlation spectra (FCS) indicating multiphoton excitation of wild-type Nef (Figure 7). The relationship between fluorescence intensity and laser power should ideally be of cubic power in case of three-photon absorption but was determined to be at the power of 2.7 here. However, since at high laser power precipitation of the sample occurred, the exact relationship was difficult to determine. To our knowledge, direct three-photon excitation of a protein has been only reported for a mutant of troponin C that contained a single tryptophan residue at a mutant site (*32*).

The shape of the autocorrelation functions revealed that myristoylation of Nef significantly influenced the diffusion of the protein in aqueous solution. From a fit of these curves the characteristic translational diffusion times τ_{diff} were calculated (Table 1), which correspond to the average times a particle spends within the $3h\nu$ excitation volume. The characteristic residence time for myristoylated Nef was almost 2-fold smaller compared to its nonmyristoylated form, which suggested that myristoylation leads to a significantly more compactly folded protein. In contrast, the diffusion times for the truncated forms (45−210 and 59−210) were only slightly smaller, which might result from an increased tendency for oligmerization as observed by analytical gel

filtration and indicated by NMR spectroscopy. However, the standard errors of the characteristic diffusion times as derived from a fit to the autocorrelation function were up to 30% and very much dependent on the initial data points measured at low correlation times τ. Overall, the FCS measurements indicated different translational diffusion times suggesting a conformational change for the myristoylated protein.

DISCUSSION

This study focused on biochemical aspects of myristoylation of the HIV-1 Nef protein. The evaluation of elution profiles from size exclusion chromatography, the antibody recognition and pattern of limited proteolytic digest, and the calculation of diffusion times from fluorescence correlation spectroscopy measurements all revealed different sizes and accessibilities in aqueous solution for the myristoylated Nef protein compared to its unmodified form. Moreover, analytical ultracentrifugation showed that unlipidated Nef existed in an equilibrium of self-associated aggregates while myristoylated Nef prevailed in a monomeric form. These data indicated structural changes within the protein upon lipidation and suggested different conformations for the membrane-bound and cytosolic form of Nef.

We first established an in vivo expression assay for Nef myristoylation in *E. coli* cells using the *N*-myristoyltransferase for coexpression and addition of myristic acid as substrate. To increase the yield of Nef protein expression, we optimized the codon usage by a change of rare codons AGG, AGA, and CTA to the corresponding more commonly used codons in *E. coli*. By this procedure, we obtained an approximately 15-fold higher expression level for the standard full-length Nef production. In particular, we could increase the expression temperature with the codon-optimized *nef* plasmid to 28 °C, which we found to be beneficial for the myristoylation reaction by the NMT. The efficiency of the myristoylation reaction was estimated to be higher than 95%; in fact, we could not observe any nonmyristoylated Nef protein by mass spectrometry. These results are in line with previous observations that coexpression of the target gene together with the NMT plus addition of 50 μM myristic acid to the expression medium clearly shifted the enzymatic reaction equilibrium toward a full myristoylation saturation (*33*). Alternatively to codon optimization, modified cell lines that supplement for rare codon usage could be used to increase the protein expression to similar levels. However, this latter strategy requires an additional antibiotic selection. The codon-optimized plasmid, in contrast, seems to be superior when an additional restraint is introduced, as would be, e.g., protein expression on minimal medium for stable isotope labeling.

Size exclusion chromatography showed that myristoylated Nef appeared of smaller size than the unmodified form, but not as small as N-terminally truncated Nef(45−210) that misses almost the entire anchor domain. Interestingly, this Nef variant showed some dimerization and higher oligomerization fractions that were not observed in the two full-length proteins. Potentially, the truncation uncovers a surface on Nef that now leads to homomer formation which otherwise is not accessible in the protein. Particularly, residues on α-helix 4 and the adjacent loop (R109−D127) have been identified previously to form the molecular basis for Nef core domain dimer and trimer associations (*34*). Furthermore, from analytical ultracentrifugation experiments the equilibirum of self-associations seemed to be changed between the myristoylated and unlipidated form of Nef. While in the sedimentation coefficient distribution the nonmyristoylated Nef appeared in an equilibrium composed of monomer, dimer, and trimer fractions with decreasing populations, the myristoylated Nef prevails in a single monomeric state. This suggested that the cytosolic nonmembrane-bound form of Nef might adopt a conformation where is stays largely monomer, while the membrane-bound form existed in a dynamic equilibrium of self-associations. In a recent report on a different Nef allele, BH10, a large aggregate made of 16 Nef molecules was observed for the unmodified form while myristoylation changed the protein to a predominantly monomeric form and small oligomers (*35*). While we similarly find monomerization upon myristoylation, these highly oligomeric structures of Nef could not be confirmed in our experiments. Since the multimer formations of Nef may hence be related to the conformation of the anchor domain or N-terminal truncations, future structural studies on the full-length protein should be performed to address this question.

Fluorescence correlation spectroscopy is perhaps the most informative technique to analyze the diffusion of a molecule in a particular environment, either in vitro or in vivo (*36*, *37*). The translational diffusion time, which is the average lateral transit time of the particles through the ellipsoidal measuring volume (<0.5 fL), relates by the diffusion coefficient and the Stokes−Einstein equation to the hydrodynamic radius of the particles. For approximately spherical particles a linear relation between the diffusion time and the hydrodynamic radius holds. Since we observed an almost 2-fold lower diffusion time for myristoylated Nef compared to the unmodified form, there should be a large difference in the overall shape of the two molecules. Only a fully flexible anchor domain in the nonlipidated protein versus a rather compact anchor domain in the myristoylated Nef may explain such differences. Hence, it is surprising that the two truncated forms (45−210 and 59−210) do not exhibit smaller diffusion times. A possible explanation could be the augmented dimerization and trimerization as described above. Alternatively, also the C-terminal flexible loop of Nef might be involved in the conformational changes in a cooperative manner and enlarge the volume by an "open" or "closed" conformation (*38*).

Multiphoton excitation (MPE) is the simultaneous absorption of two or more long-wavelength photons to excite the lowest singlet state of a fluorophore (*39*−*41*). Specially designed MPE chromophores have gained biological importance since they allow noninvasive investigations of biological processes within the subfemtoliter volume (*42*). Since in our experiments Nef was not labeled with any conjugation unit, the most likely explanation for the observed fluorescence emission is three-photon excitation due to confined tryptophan residues within the protein, as has been suggested before for human serum albumin (*43*). To date, the complex photophysics of proteins containing tryptophans is explained by an ionization/recombination mechanism of the excited states (*44*). This involves ionization of the excited tryptophan residues, due to the collisional transfer of an electron to the side chain of the neighboring residue (*45*). A similar

mechanism in which the chromophore is converted into a new fluorescent species could be responsible for multiphoton excitation of tryptophans. Since the intensity of the three-photon excitation of Nef is strong, it is possible to assume that geometrical constraints of the tryptophan assembly within the Nef core domain structure enhance the observed multiphoton processes.

Our data suggest that the lipidation of Nef might induce a folding of the hydrophobic fatty acid to the core domain structure while the anchor domain of the unmodified form is rather flexible. This transition may include even additional conformational changes in the C-terminal flexible loop of Nef and induce formation of secondary structure elements in otherwise flexible regions. An extension of helical structure elements upon myristoylation was indeed observed for the anchor domain of Nef (*24*). A compact globular structure of myristoylated Nef that is thought to reflect the cytosolic conformation versus a loose unmodified form that may represent the membrane-associated state when the myristate in inserted into the lipid bilayer would suggest some kind of dynamic regulation. Such model has been previously quoted to explain the complex activities of Nef (*38*) and was correlated with the exposure of a cluster of negatively charged residues close to the dileucine-based internalization motif in the membrane-bound form of Nef (*46*). Myristoylation switches have been observed, e.g., for the small GTP-binding protein Arf1, the Marcks proteins, or recoverin (*47*−*49*). Here, the GDP to GTP exchange, phosphorylation, or calcium binding, respectively, induces conformational changes that lead to exposure of the lipid moiety and subsequently direct membrane attachment. While Nef is missing such enzymatic activity, it could be regulated by a kind of autoinhibitory myristoyl switch mechanism, such as the c-Abl tyrosine kinase, which has been recently found to regulate docking and accessibility of the SH2 domain by a combined myristoyl/phosphotyrosine switch mechanism (*50*). Alternatively, interacting proteins of Nef that actively sense for a conformational change upon myristoylation could act as effectors for membrane association. Such differences in recognition have been recently reported for the interaction with calmodulin in vivo and assigned to the N-terminal residues in Nef (*51*). Another regulation mechanism was identified for the HIV-1 matrix protein that shifted between monomer and trimer formations by entropic modulation of preexisting equilibrium states (*52*). For Nef, its various interacting proteins and the interplay with its C-terminal flexible loop may contribute to the regulation of its cytosol−membrane attachment equilibrium. Further studies will be directed on the structural properties of Nef and its membrane attachment in cells.

ACKNOWLEDGMENT

We thank Diana Ludwig for expert technical assistance, Michael Alexander for expression tests on codon-optimized Nef constructs, Vanessa Laumann for ESI mass spectrometry, and Oliver Fackler and Roger Goody for stimulating discussions. A plasmid coding for the human *N*-myristoyltransferase is a kind gift of Jeff Gordon, Washington University, St. Louis, MO. We gratefully acknowledge the Nef-directed antibody from Mark Harris, University of Leeds.

REFERENCES

1. Resh, M. D. (1996) Regulation of cellular signalling by fatty acid acylation and prenylation of signal transduction proteins, *Cell. Signalling 8*, 403−412.
2. Greene, W. C., and Peterlin, B. M. (2002) Charting HIV's remarkable voyage through the cell: Basic science as a passport to future therapy, *Nat. Med. 8*, 673−680.
3. Renkema, G. H., and Saksela, K. (2000) Interactions of HIV-1 NEF with cellular signal transducing proteins, *Front. Biosci. 5*, D268−D283.
4. Fackler, O. T., and Baur, A. S. (2002) Live and let die: Nef functions beyond HIV replication, *Immunity 16*, 493−497.
5. Geyer, M., Fackler, O. T., and Peterlin, B. M. (2001) Structure−function relationships in HIV-1 Nef, *EMBO Rep. 2*, 580−585.
6. Janardhan, A., Swigut, T., Hill, B., Myers, M. P., and Skowronski, J. (2004) HIV-1 Nef binds the DOCK2-ELMO1 complex to activate Rac and inhibit lymphocyte chemotaxis, *PLoS Biol. 2*, E6.
7. Renkema, G. H., Manninen, A., Mann, D. A., Harris, M., and Saksela, K. (1999) Identification of the Nef-associated kinase as p21-activated kinase 2, *Curr. Biol. 9*, 1407−1410.
8. Fackler, O. T., Luo, W., Geyer, M., Alberts, A. S., and Peterlin, B. M. (1999) Activation of Vav by Nef induces cytoskeletal rearrangements and downstream effector functions, *Mol. Cell 3*, 729−739.
9. Witte, V., Laffert, B., Rosorius, O., Lischka, P., Blume, K., Galler, G., Stilper, A., Willbold, D., D'Aloja, P., Sixt, M., Kolanus, J., Ott, M., Kolanus, W., Schuler, G., and Baur, A. S. (2004) HIV-1 Nef mimics an integrin receptor signal that recruits the polycomb group protein Eed to the plasma membrane, *Mol. Cell 13*, 179−190.
10. Janvier, K., Craig, H., Hitchin, D., Madrid, R., Sol-Foulon, N., Renault, L., Cherfils, J., Cassel, D., Benichou, S., and Guatelli, J. (2003) HIV-1 Nef stabilizes the association of adaptor protein complexes with membranes, *J. Biol. Chem. 278*, 8725−8732.
11. Geyer, M., Yu, H., Mandic, R., Linnemann, T., Zheng, Y. H., Fackler, O. T., and Peterlin, B. M. (2002) Subunit H of the V-ATPase binds to the medium chain of adaptor protein complex 2 and connects Nef to the endocytic machinery, *J. Biol. Chem. 277*, 28521−28529.
12. Madrid, R., Janvier, K., Hitchin, D., Day, J., Coleman, S., Noviello, C., Bouchet, J., Benmerah, A., Guatelli, J., and Benichou, S. (2005) Nef-induced alteration of the early/recycling endosomal compartment correlates with enhancement of HIV-1 infectivity, *J. Biol. Chem. 280*, 5032−5044.
13. Rose, J. J., Janvier, K., Chandrasekhar, S., Sekaly, R. P., Bonifacino, J. S., and Venkatesan, S. (2005) CD4 down-regulation by HIV-1 and simian immunodeficiency virus (SIV) Nef proteins involves both internalization and intracellular retention mechanisms, *J. Biol. Chem. 280*, 7413−7426.
14. Harris, M. (1995) The role of myristoylation in the interactions between human immunodeficiency virus type I Nef and cellular proteins, *Biochem. Soc. Trans. 23*, 557−561.
15. Resh, M. D. (1999) Fatty acylation of proteins: new insights into membrane targeting of myristoylated and palmitoylated proteins, *Biochim. Biophys. Acta 1451*, 1−16.
16. Geyer, M., and Peterlin, B. M. (2001) Domain assembly, surface accessibility and sequence conservation in full length HIV-1 Nef, *FEBS Lett. 496*, 91−95.
17. Niederman, T. M., Hastings, W. R., and Ratner, L. (1993) Myristoylation-enhanced binding of the HIV-1 Nef protein to T cell skeletal matrix, *Virology 197*, 420−425.
18. Kaminchik, J., Margalit, R., Yaish, S., Drummer, H., Amit, B., Sarver, N., Gorecki, M., and Panet, A. (1994) Cellular distribution of HIV type 1 Nef protein: identification of domains in Nef required for association with membrane and detergent-insoluble cellular matrix, *AIDS Res. Hum. Retroviruses 10*, 1003−1010.
19. Coates, K., Cooke, S. J., Mann, D. A., and Harris, M. P. G. (1997) Protein kinase C-mediated phosphorylation of HIV-I nef in human cell lines, *J. Biol. Chem. 272*, 12289−12294.
20. Fackler, O. T., Kienzle, N., Kremmer, E., Boese, A., Schramm, B., Klimkait, T., Kucherer, C., and Mueller-Lantzsch, N. (1997) Association of human immunodeficiency virus Nef protein with actin is myristoylation dependent and influences its subcellular localization, *Eur. J. Biochem. 247*, 843−851.

21. Grzesiek, S., Bax, A., Hu, J. S., Kaufman, J., Palmer, I., Stahl, S. J., Tjandra, N., and Wingfield, P. T. (1997) Refined solution structure and backbone dynamics of HIV-1 Nef, *Protein Sci. 6*, 1248−1263.
22. Lee, C. H., Saksela, K., Mirza, U. A., Chait, B. T., and Kuriyan, J. (1996) Crystal structure of the conserved core of HIV-1 Nef complexed with a Src family SH3 domain, *Cell 85*, 931−942.
23. Arold, S., Franken, P., Strub, M. P., Hoh, F., Benichou, S., Benarous, R., and Dumas C. (1997) The crystal structure of HIV-1 Nef protein bound to the Fyn kinase SH3 domain suggests a role for this complex in altered T cell receptor signaling, *Structure 5*, 1361−1372.
24. Geyer, M., Munte, C. E., Schorr, J., Kellner, R., and Kalbitzer, H. R. (1999) Structure of the anchor-domain of myristoylated and non-myristoylated HIV-1 Nef protein, *J. Mol. Biol. 289*, 123−138.
25. Duronio, R. J., Reed, S. I., and Gordon, J. I. (1992) Mutations of human myristoyl-CoA:protein N-myristoyltransferase cause temperature-sensitive myristic acid auxotrophy in *Saccharomyces cerevisiae*, *Proc. Natl. Acad. Sci. U.S.A. 89*, 4129−4133.
26. Lebowitz, J., Lewis, M. S., and Schuck, P. (2002) Modern analytical ultracentrifugation in protein science: a tutorial review, *Protein Sci. 11*, 2067−2079.
27. Schulte, A., Czudnochowski, N., Barboric, M., Schonichen, A., Blazek, D., Peterlin, B. M., and Geyer, M. (2005) Identification of a cyclin T-binding domain in Hexim1 and biochemical analysis of its binding competition with HIV-1 Tat, *J. Biol. Chem. 280*, 24968−24977.
28. Kane, J. F. (1995) Effects of rare codon clusters on high-level expression of heterologous proteins in *Escherichia coli*, *Curr. Opin. Biotechnol. 6*, 494−500.
29. Franco, M., Chardin, P., Chabre, M., and Paris, S. (1996) Myristoylation-facilitated binding of the G protein ARF1GDP to membrane phospholipids is required for its activation by a soluble nucleotide exchange factor, *J. Biol. Chem. 271*, 1573−1578.
30. Freund, J., Kellner, R., Houthaeve, T., and Kalbitzer, H. R. (1994) Stability and proteolytic domains of Nef protein from human immunodeficiency virus (HIV) type 1, *Eur. J. Biochem. 221*, 811−819.
31. Opitz, N., Rothwell, P. J., Oeke, B., and Schwille, P. (2003) Single molecule FCS-based oxygen sensor (O-2-FCSensor): a new intrinsically calibrated oxygen sensor utilizing fluorescence correlation spectroscopy (FCS) with single fluorescent molecule detection sensitivity, *Sens. Actuators, B 96*, 460−467.
32. Gryczynski, I., Malak, H., Lakowicz, J. R., Cheung, H. C., Robinson, J., and Umeda, P. K. (1996) Fluorescence spectral properties of troponin C mutant F22W with one-, two-, and three-photon excitation, *Biophys. J. 71*, 3448−3453.
33. Farazi, T. A., Waksman, G., and Gordon, J. I. (2001) The biology and enzymology of protein N-myristoylation, *J. Biol. Chem. 276*, 39501−39504.
34. Arold, S., Hoh, F., Domergue, S., Birck, C., Delsuc, M. A., Jullien, M., and Dumas, C. (2000) Characterization and molecular basis of the oligomeric structure of HIV-1 Nef protein, *Protein Sci. 9*, 1137−1148.
35. Dennis, C. A., Baron, A., Grossmann, J. G., Mazaleyrat, S., Harris, M., and Jaeger, J. (2005) Co-translational myristoylation alters the quaternary structure of HIV-1 Nef in solution, *Proteins 60*, 658−669.
36. Diaspro, A. (2002) *Confocal and two-photon microscopy*, Wiley-Liss, New York.
37. Bacia, K., and Schwille, P. (2003) A dynamic view of cellular processes by in vivo fluorescence auto- and cross-correlation spectroscopy, *Methods 29*, 74−85.
38. Arold, S. T., and Baur, A. S. (2001) Dynamic Nef and Nef dynamics: how structure could explain the complex activities of this small HIV protein, *Trends Biochem. Sci. 26*, 356−363.
39. Denk, W., Strickler, J. H., and Webb, W. W. (1990) Two-photon laser scanning fluorescence microscopy, *Science 248*, 73−76.
40. Zipfel, W. R., Williams, R. M., and Webb, W. W. (2003) Nonlinear magic: multiphoton microscopy in the biosciences, *Nat. Biotechnol. 21*, 1369−1377.
41. Lakowicz, J. R., Gryczynski, I., and Gryczynski, Z. (1999) High throughput screening with multiphoton excitation, *J. Biomol. Screen. 4*, 355−362.
42. He, G. S., Markowicz, P. P., Lin, T. C., and Prasad, P. N. (2002) Observation of stimulated emission by direct three-photon excitation, *Nature 415*, 767−770.
43. Lakowicz, J. R., and Gryczynski, I. (1992) Tryptophan fluorescence intensity and anisotropy decays of human serum albumin resulting from one-photon and two-photon excitation, *Biophys. Chem. 45*, 1−6.
44. Hudson, B. S. (1999) An ionization/recombination mechanism for complexity of the fluorescence of tryptophan in proteins, *Acc. Chem. Res. 32*, 297−300.
45. Nishimura, G., and Kinjo, M. (2003) Visible emission of a photoproduct from tryptophan solution induced by multiphoton excitation: An investigation by intensity fluctuation analysis, *J. Phys. Chem. B 107*, 6012−6017.
46. Geyer, M., Fackler, O. T., and Peterlin, B. M. (2002) Subunit H of the V-ATPase involved in endocytosis shows homology to beta-adaptins, *Mol. Biol. Cell 13*, 2045−2056.
47. Antonny, B., Beraud-Dufour, S., Chardin, P., and Chabre, M. (1997) N-terminal hydrophobic residues of the G-protein ADP-ribosylation factor-1 insert into membrane phospholipids upon GDP to GTP exchange, *Biochemistry 36*, 4675−4684.
48. McLaughlin, S., and Aderem, A. (1995) The myristoyl-electrostatic switch: a modulator of reversible protein-membrane interactions, *Trends Biochem. Sci. 20*, 272−276.
49. Ames, J. B., Ishima, R., Tanaka, T., Gordon, J. I., Stryer, L., and Ikura, M. (1997) Molecular mechanics of calcium-myristoyl switches, *Nature 389*, 198−202.
50. Hantschel, O., Nagar, B., Guettler, S., Kretzschmar, J., Dorey, K., Kuriyan, J., and Superti-Furga, G. (2003) A myristoyl/phosphotyrosine switch regulates c-Abl, *Cell 112*, 845−857.
51. Matsubara, M., Jing, T., Kawamura, K., Shimojo, N., Titani, K., Hashimoto, K., and Hayashi, N. (2005) Myristoyl moiety of HIV Nef is involved in regulation of the interaction with calmodulin in vivo, *Protein Sci. 14*, 494−503.
52. Tang, C., Loeliger, E., Luncsford, P., Kinde, I., Beckett, D., and Summers, M. F. (2004) Entropic switch regulates myristate exposure in the HIV-1 matrix protein, *Proc. Natl. Acad. Sci. U.S.A. 101*, 517−522.

BI052052C